Study of dopant distribution in Cr4+:YAG transparent ceramics and its use as passively Q-switching media in Nd:YAG laser delivering 38 mJ per pulse

Camille Perrière, Rémy Boulesteix, Alexandre Maitre, Benjamin Forestier, Alain Jalocha, Alain Brenier

Optical Materials: X

Study of dopant distribution in Cr4+:YAG transparent ceramics and its use as passively Q-switching media in Nd:YAG laser delivering 38 mJ per pulse.

--Manuscript Draft--

Manuscript Number:	OMX-D-21-00074
Article Type:	VSI: Optical Ceramic Materials
Keywords:	YAG; tetravalent chromium; transparent ceramics; saturable absorber; laser
Abstract:	In this work, the role of elaboration parameters (i.e. chemical composition and heat treatments) of Cr:YAG ceramics on their microstructural, optical and laser properties was investigated. Transparent ceramics were manufactured by solid-state reactive sintering under vacuum. Spatial distribution of sintering additives and luminescent dopant (Ca, Mg, Cr 3+ and Cr 4+) has been determined by coupling TEM, LSFI and NanoSIMS complementary techniques. Ca and Mg were found to segregate at grain boundaries whereas Cr appears to be homogenously distributed in Cr:YAG ceramics. Samples were used as saturable absorber of Nd:YAG laser and exhibited good optical properties, i.e. saturation fluence of 4500 J.m -2 , laser pulse energy of 38.8 mJ with pulse duration of 45 ns.

Highlights

- Cr,Ca,Mg:YAG transparent ceramics of high optical quality were manufactured by the solid-state reaction sintering method
- Ca and Mg segregate at grain boundaries whereas there is no Cr segregation
- Cr (Cr^{3+} or Cr^{4+}) is homogeneously distributed in Cr,Ca,Mg:YAG transparent ceramics
- Cr,Ca,Mg:YAG transparent ceramics allow delivering laser pulse energy around 39 mJ and peak power about 0.8 MW at 1064 nm

Study of dopant distribution in Cr^{4+}:YAG transparent ceramics and its use as passively Q-switching media in Nd:YAG laser delivering 38 mJ per pulse.

Camille Perrière[1,2], Rémy Boulesteix[1,2*], Alexandre Maître[1,2], Benjamin Forestier[3], Alain Jalocha[2,3], Alain Brenier[4]

[1] Univ. Limoges, IRCER, UMR CNRS 7315, F-87068 Limoges, FRANCE

[2] LCTL, IRCER, UMR CNRS 7315, F-87068 Limoges, FRANCE

[3] CILAS, F-45063 Orléans, FRANCE

[4] Univ. Claude Bernard Lyon 1, ILM, UMR CNRS 5306, F-69622 Lyon, FRANCE

(*) Author to whom the correspondence should be addressed

Tel.: 0587502345 E-mail: remy.boulesteix@unilim.fr

Abstract

In this work, the role of elaboration parameters (*i.e.* chemical composition and heat treatments) of Cr:YAG ceramics on their microstructural, optical and laser properties was investigated. Transparent ceramics were manufactured by solid-state reactive sintering under vacuum. Spatial distribution of sintering additives and luminescent dopant (Ca, Mg, Cr^{3+} and Cr^{4+}) has been determined by coupling TEM, LSFI and NanoSIMS complementary techniques. Ca and Mg were found to segregate at grain boundaries whereas Cr appears to be homogenously distributed in Cr:YAG ceramics. Samples were used as saturable absorber of Nd:YAG laser and exhibited good optical properties, *i.e.* saturation fluence of 4500 $J.m^{-2}$, laser pulse energy of 38.8 mJ with pulse duration of 45 ns.

Keywords: YAG; tetravalent chromium; transparent ceramics; saturable absorber; laser

1. Introduction

Q-switched pulsed lasers are capable to deliver short light pulses and high peak power. With Q-switching method, giant laser pulses can be generated by allowing the pumping process to buildup a population inversion and gain inside the laser cavity without oscillations, which are larger than the normal values under free-running operation. This type of lasers can be useful for multiple applications, like laser marking, laser medicine, designation or telemetry. The Q-switching technology can be generated by an electro-optical [1] or acousto-optical [2] device (actively Q-switched methods) or by a saturable absorber (passively Q-switched method). The last one operates without any external power supply. In consequence, it presents various advantages, such as simple design, compactness, and low cost [3].

Chromium IV doped Yttrium Aluminum Garnet (Cr^{4+}:YAG or Cr^{4+}:$Y_3Al_5O_{12}$) is attracting a great attention due to its good properties as saturable absorber (SA) for laser emitting around 1 µm [4]. It is mainly used as SA with YAG doped Nd^{3+} or Yb^{3+} [5,6], owing to absorption bands of Cr^{4+} ion ranging from 800 nm to 1200 nm. The additional advantages of the Cr^{4+} ion is its relatively large absorption cross-section and low saturation fluence of around 1064 nm. Also, the Cr^{4+}:YAG has excellent thermo-mechanical and chemical properties, which make this material a reliable and stable optical component even at high photon fluence. Cr^{4+}:YAG was used in several studies in single crystal form [5,7], but it showed output power limitation because of a low solid solubility of Cr^{4+} ions during single crystal growth and relatively low Cr^{3+} to Cr^{4+} conversion efficiency [8–10]. In fact, chromium-doped YAG originally include Cr in its trivalent state. Simultaneous doping of the YAG matrix with Ca^{2+} and Mg^{2+} cations has been shown to be effective in changing chromium oxidation state ~~to~~ from +III to +IV and maintain charge balance in YAG structure [11][12]. Cr^{4+}:YAG, due to its isotropic crystalline structure, can be also elaborated in the form of transparent polycristalline ceramics. Ceramic processes provide many advantages over single crystal ones such as lower temperatures and shorter production cycle. Moreover, they allow the development of large size pieces and components with complex architectures thank to flexible ceramic processes [13,14]. Nevertheless, the elaboration of transparent ceramics is not easy and necessitates a perfect control of the process in order to avoid any residual defects

impairing the transparency of the material by light diffusion. With this aim, some studies have already focused on the role of Ca^{2+} and Mg^{2+} as sintering aids [15–25]. Also, the influence of process parameters (sintering aids content, annealing temperature, etc.) on the Cr^{4+}:YAG ceramics properties has been already considered [26–32]. As a result, laser performance of Cr^{4+}:YAG ceramics used as SA with Nd:YVO_4 amplifier medium has been investigated and demonstrated a maximum output power of 100.8 mW at 1064 nm under an incident pump power of 2.14 W [10]. Other authors have obtained a pulsed Nd:YAG laser at 1064 nm using Cr^{4+}:YAG ceramics as SA with 20 µJ per pulse [28] or 190 W and 20 ns laser pulse [30].

Up to now, none of the studies have taken in consideration the homogeneity of chromium and chromium conversion efficiency at nano-, micro- and macroscopic scale. Thus, this paper proposes to study the microstructural features and distribution of Cr^{3+} and Cr^{4+} in Cr:YAG transparent ceramics after sintering as a function of process parameters (*i.e.* chemical composition and atmosphere used during thermal treatment) by using TEM (Transmission Electron Microscopy), LSFI (Laser Sheet Fluorescence Imaging) and nanoSIMS (Nano-Secondary Ion Mass Spectrometry) techniques. NanoSIMS allows obtaining the distribution of dopants (Ca, Mg and Cr) at nanometric scale (*i.e.* < 5 µm) whereas LSFI allows determining the spatial distribution of luminescent Cr^{4+} ions at micro- and macroscopic scale (*i.e.* > 10 µm). Finally, we also report in this paper the optical and laser properties of Cr^{4+}:YAG transparent ceramics used as SA of high peak energy Nd:YAG laser at 1064 nm.

2. Experimental procedure

2.1. Elaboration of ceramics

Cr:YAG transparent ceramics were elaborated by solid-state reactive sintering according to the following process. Aqueous suspensions were prepared using high purity powders of α-Al_2O_3 (Baikowski, Annecy, France), Y_2O_3 (Solvay, La Rochelle, France), Cr_2O_3 (Alfa Aesar, Kandel, Germany), SiO_2 (Alfa Aesar, Kandel, Germany), MgO (US Research Nanomaterials, Houston, USA) and $CaCO_3$ (US Research Nanomaterials, Houston, USA) as raw materials and a commercial dispersant (Dolapix CE64, Zschimmer & Schwartz, Lahnstein, Germany). TEM micrographs of powders used in

this study are presented in *Figure 1*. Powder particles are well crystallized, weakly aggregated with submicrometric sizes.

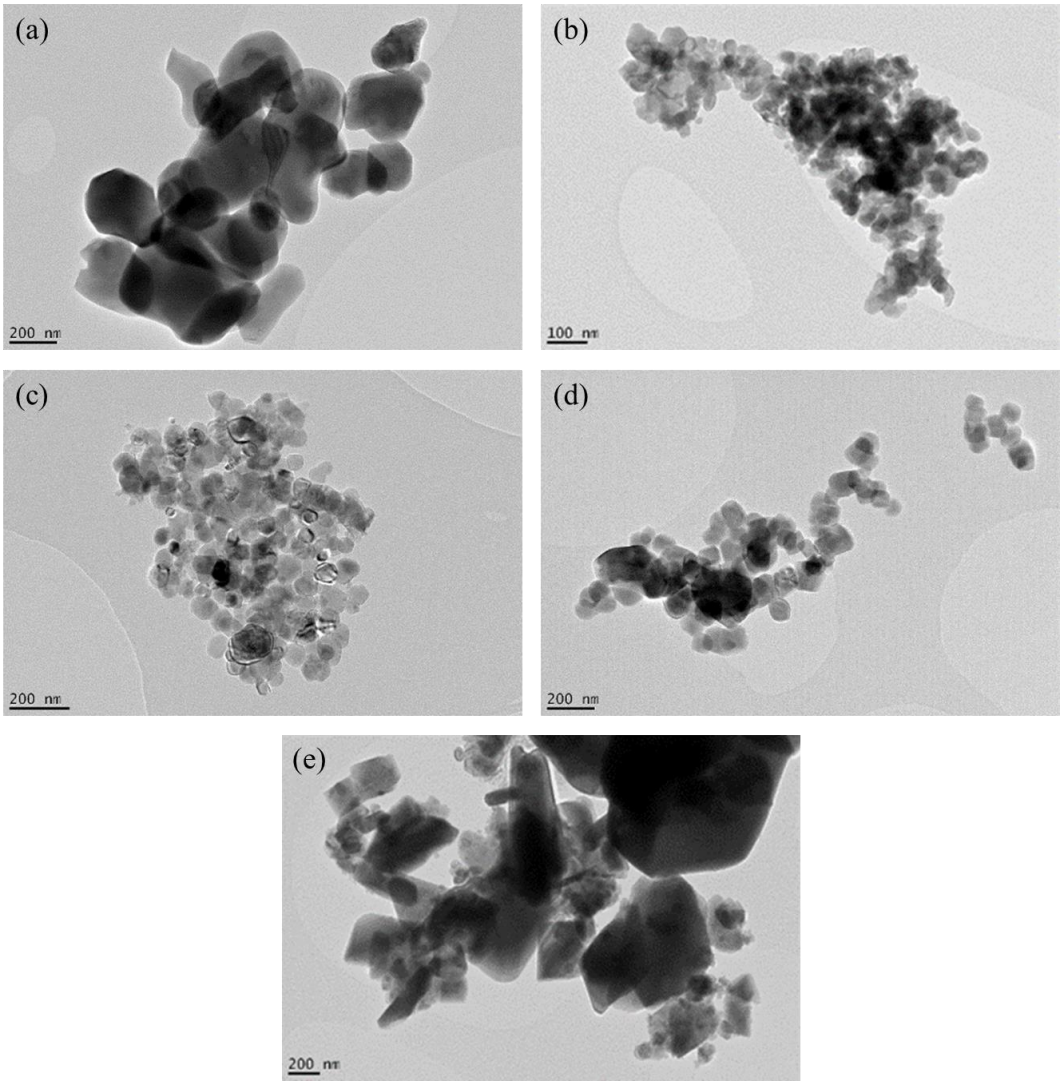

Figure 1 : TEM micrographs of Al_2O_3 (a), Y_2O_3 (b), MgO (c), $CaCO_3$ (d) and Cr_2O_3 (e) raw powders.

Primary powders were mixed together according to the desired stoichiometric ratio for obtaining Cr:YAG after reaction. Finally, samples were shaped by pressure casting from as-obtained slurries as described elsewhere [33]. Obtained green bodies were dried at room temperature overnight then debinded under air at a temperature of 700°C to remove organic residues. Finally samples were subjected to reactive-sintering at 1700°C for 10 h under vacuum in a tungsten mesh-heated furnace ($P \leq 10^{-4}$ Pa) to provide fully dense material. Samples were finally annealed under air at temperatures ranging from 1200°C to 1300°C for 10 h to change the valence +III to +IV of chromium ions.

According to the literature [22,34,35], the general formula obtained for totally substituted (Cr,Ca,Mg,Si):YAG ceramics was assumed to be $Y_{3-x}Ca_xAl_{5-y-z-t}Mg_yCr_zSi_tO_{12}$. In our study, powders were blended together in stoichiometric proportions to form after thermal treatment 0.1at.%Cr:YAG ceramics with various dopant concentrations and annealing temperatures in order to address their effect on samples optical properties. Samples characteristics were summarized in Table 1 and corresponding view is reported in Figure 2.

Table 1: Summary of 0.1at.%Cr:YAG samples characteristics.

Sample Ref.	Chemical formula	Ca conc. (at.%)	Mg conc. (at.%)	Si conc. (at.%)	Annealing temperature (°C)
Single-crystal	$Y_{2.988}Ca_{0.012}Al_{4.992}Mg_{0.003}Cr_{0.005}O_{12}$	0.4	0.06	0	-
CaMg1200	$Y_{2.9952}Ca_{0.0048}Al_{4.9937}Mg_{0.002}Cr_{0.005}O_{12}$	0.16	0.04	0	1200
CaMg1300	$Y_{2.9952}Ca_{0.0048}Al_{4.9937}Mg_{0.002}Cr_{0.005}O_{12}$	0.16	0.04	0	1300
CaMgSi1300	$Y_{2.9952}Ca_{0.0048}Al_{4.9905}Mg_{0.002}Cr_{0.005}Si_{0.0025}O_{12}$	0.16	0.04	0.05	1300

All samples present a rather good transparent coefficient but different colors (*i.e.* different ratios between Cr^{3+} (green) and Cr^{4+} (brown)) were obtained depending on doping and annealing conditions.

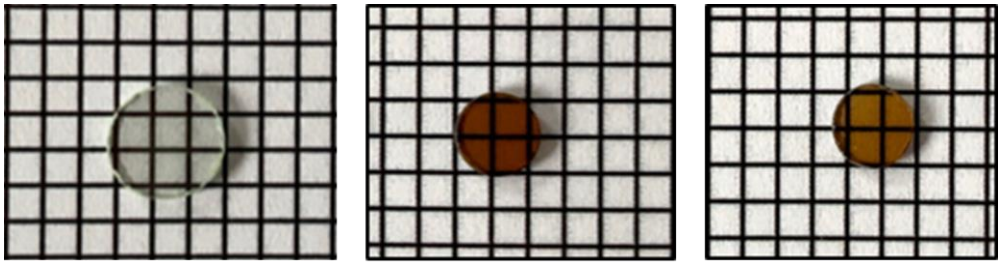

Figure 2: View of 0.1at.% Cr:YAG as sintered (a) and annealed samples (CaMg1300 (b) and CaMgSi1300 (c))

2.2. Structural and microstructural characterizations

The chemical and microstructural homogeneity of green and sintered samples was analyzed by scanning electron microscopy (FE-SEM, LEO 1530 VP, Zeiss, Germany) coupled with EDS chemical analysis. Before SEM observations of sintered samples, surface samples were polished and thermally

etched at a temperature 200°C below the sintering temperature. Grain size distribution and average grain size of sintered ceramics were determined by image analysis technique using ImageJ software.

Crystalline phases of sintered parts were identified by X-ray diffraction analyses (D8, Bruker, Karmsruhe, Germany) using CuKα radiation. $CuK\alpha_2$ radiation contribution was removed and obtained diagrams were in indexed with DIFFRACplus EVA™ software and the PDFmain™ database.

2.3. *Optical and laser properties characterizations*

In-line transmittance measurements of the Cr^{4+}:YAG mirror polished samples were realized with a UV-visible spectrometer Cary 5000 (Varian, USA). Cr^{4+} concentration was deduced by methodology described elsewhere [36] that used the relation:

$$[Cr^{4+}] = \frac{K}{\sigma} \quad (1)$$

where k is the absorption coefficient at 1064 nm and $\sigma = 5.04 \cdot 10^{-19}$ cm^2 is the Cr^{4+}:YAG absorption cross-section at 1064 nm.

The distribution of the Cr^{4+} ions in the Cr-doped YAG samples was visualized by LSFI (see [36] for more details). In this technique, Cr^{4+} fluorescence is excited by a laser and is imaged on a camera behind the sample. The tetrahedral site Cr^{4+} fluorescence was selected close to the maximum intensity of the $^3T_2 \rightarrow {}^3A_2$ transition with a 1400 nm interference filter (10 nm FWHM). It was detected by a Xeva 1.7-640 InGaAs camera from Xenics, cooled down to 263 K by a Pelletier thermoelectric cooler. The number of pixels was 640 x 512 and the pixel size was 20 µm. The excitation was provided by a 1064 nm Nd:YAG laser.

Then, the saturation fluence of Cr^{4+}:YAG ceramic was estimated on a laser system presented in Figure 3. The Cr^{4+}:YAG ceramic components were in cylindrical form with 5 mm diameter and 0.7 mm of thicknesses. They were coated with antireflective film (AR) at 1054-1074 nm and 1320 nm.

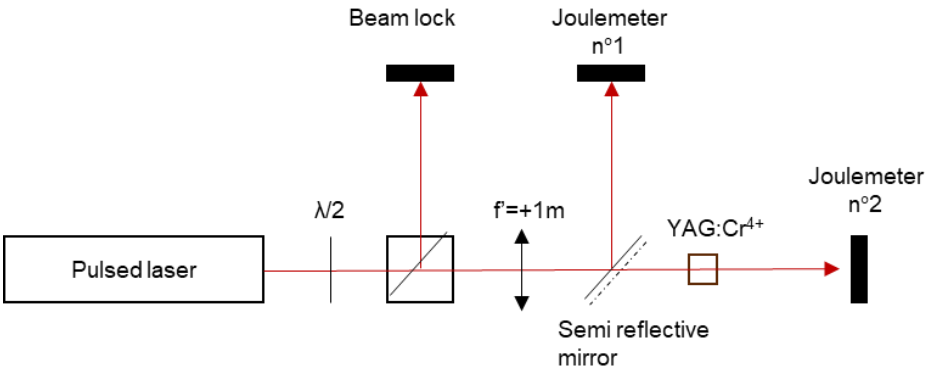

Figure 3: Schematic diagram of laser experiments for measuring Cr^{4+}:YAG saturation fluence.

According to previous works from Kalisky [7] and others, the saturable absorber has ground-state absorption and excited state absorption (ESA) cross-sections, σ_{gs} and σ_{es}; respectively. At high fluence, there is a saturation of the optical transition as a result of the ground-state bleaching, and this results in high transmission of the optical signal. Nevertheless, as many other solids used as saturable absorber, Cr^{4+}:YAG is not fully bleached and have a residual absorption which is attributed to ESA. Therefore their saturation transmission has a maximum value, T_{max}. The ratio between the ground-state absorption and ESA cross-sections is given by:

$$\frac{\sigma_{gs}}{\sigma_{es}} = \frac{ln(T_0)}{ln(T_{max})} \tag{2}$$

Under suitable approximations (see for more details [7]), the measured transmittance is a function of the input energy fluence and the saturation fluence according to modified Frantz–Nodvik equation [37]:

$$T_N = \frac{F_{sat}}{F_{i,\lambda}} ln\left(1 + \left(exp\left(\frac{F_{i,\lambda}}{F_{sat}}\right) - 1\right) T_0^*\right) t_{ESA} \tag{3}$$

where T_N is the measured lossy transmittance in the absence of the ESA, $F_{i,\lambda}$ is the input incident energy fluence at a given wavelength λ, F_{sat} is the saturation fluence, T_0^* is the small-signal transmittance in the absence of ESA and t_{ESA} is a correction factor. From Eq.(3), there are two limiting cases for the transmission of the saturable absorber: $T_N = T_0 = T_0^* t_{ESA}$ for low fluence and $T_N = T_{max} = t_{ESA}$ for high fluence. Nevertheless, in experimental conditions, one has also to consider the shape of the incident

beam to adapt the determination of deposited light energy. Thus, in this study, the analytical approximation to the solution of the Frantz–Nodvik equation in the presence of ESA for a slow saturable absorber given by Eq.(4) will be used for the determination of F_{sat}, T_0 and T_{max} parameters [38].

$$T_E = T_0 + \frac{(T_N - T_0)}{1 - T_0}(T_{max} - T_0) \quad (4)$$

where T_E is the measured transmittance as a function of fluence and T_N is the solution to the Frantz–Nodvik equation given by Eq(3). This approximation was already successfully used to predict the saturation behavior of a saturable absorber with T_0 = 60% and T_{max} = 90% (*i.e.* the case of samples characterized in this study) [38]. From this equation, it is possible to determine the output energy (measured experimentally by a power meter) from the shape of the incident beam in X,Y Cartesian coordinates as described by:

$$E_{out} = \iint_{X,Y=-\infty}^{X,Y=+\infty} I_{in,(X,Y)} \cdot T(I_{in,(X,Y)}) \cdot dX \cdot dY \quad (5)$$

$$Eout = X,Y=-\infty X,Y=+\infty Iin,X,Y \cdot T(Iin,X,Y) \cdot dX \cdot dY \quad (5)$$

should yield values of F_{sat}, T_0 and T_{max}.

Finally, the laser performance of Cr^{4+}:YAG ceramic used as SA of a Nd:YAG laser was measured. Laser cavity was pumped in longitudinal mode by laser diodes at 808 nm. The classical values obtained with comparable Cr^{4+}:YAG single-crystal were a saturation fluence of 2730 $J.m^{-2}$, laser pulse energy of 49 mJ with pulse duration of 16 ns.

3. Results

3.1. *Structural, microstructural and chemical analyses of sintered samples*

After sintering, annealing and polishing (view of samples in Figure 2), samples were first characterized in terms of structure and microstructure. XRD diagrams were reported in Figure 4 and show that samples are single-phased and composed of garnet phase.

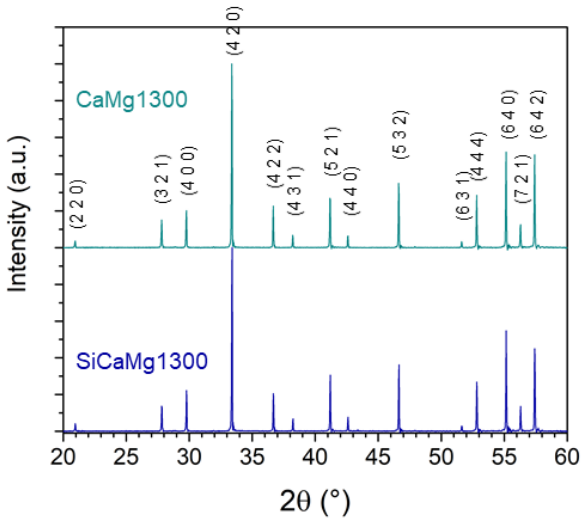

Figure 4: XRD diagrams of sintered samples (PDF card – 00-033-0040).

Secondly, SEM observations (Figure 5) were performed on samples surface showing their homogeneous and small grain size (*i.e.* mean diameter lower than 3 µm). Samples are almost pore-free and impurity-free. Also, very limited effect of initial composition (*i.e.* Si incorporation) is observed on grain size distribution. Mean grains diameter is in fact close to 2.40 µm and 2.87 µm for CaMg1300 and CaMgSi1300 samples, respectively.

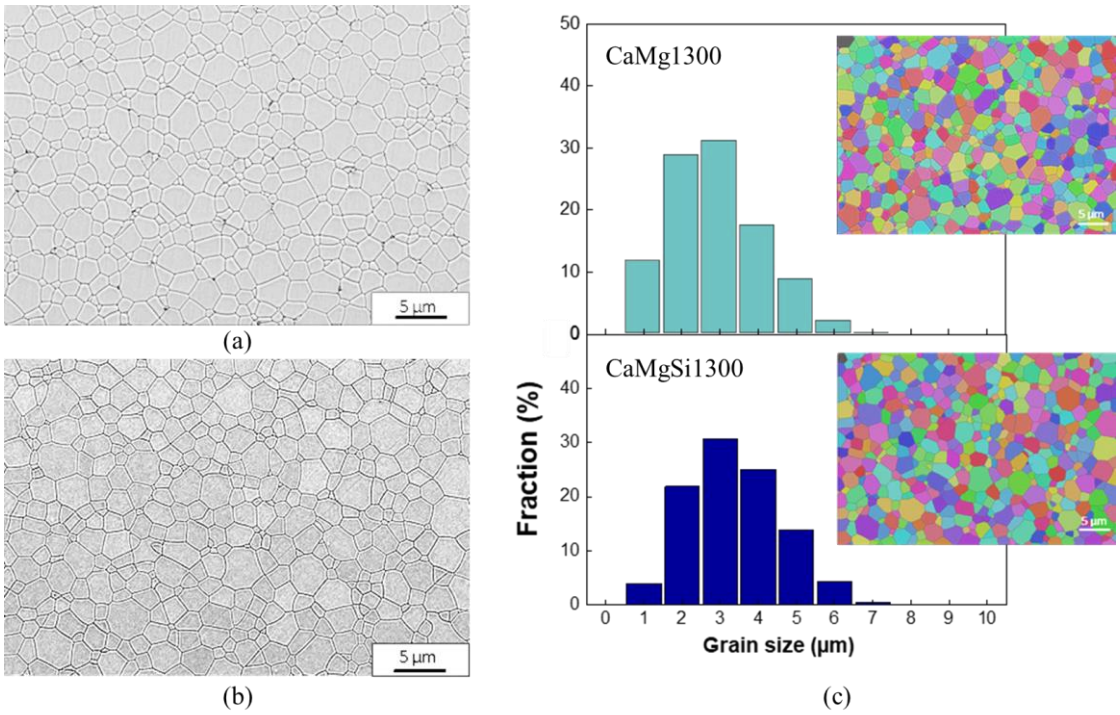

Figure 5: SEM micrographs of sintered samples CaMg1300 (a), CaMgSi1300 (b) and corresponding grain size distributions (c).

Samples were then observed at nanometric scale thanks to TEM (Figure 6). Grains are clearly visible with similar size already observed by SEM (*i.e.* 1-5 µm in diameter) and appear well crystallized. No crystalline or amorphous layers were observed by High-resolution TEM analyses at grain boundaries (Figure 6b). Nevertheless, strong Ca segregation was detected in STEM mode (Figure 6c). Such analyses are not fully quantitative and give only an estimation of Ca content at grain boundaries. From these results, a good estimation of the thickness of grain boundary enriched in Ca was obtained, *i.e.* 10 nm. By taking into consideration the mean grains diameter of Cr:YAG ceramics around 2.5 µm, it can be calculated that the volume of grain boundaries enriched in Ca represents less than 1% of the total sample volume. From STEM analyses, no Cr or Mg segregation was detected.

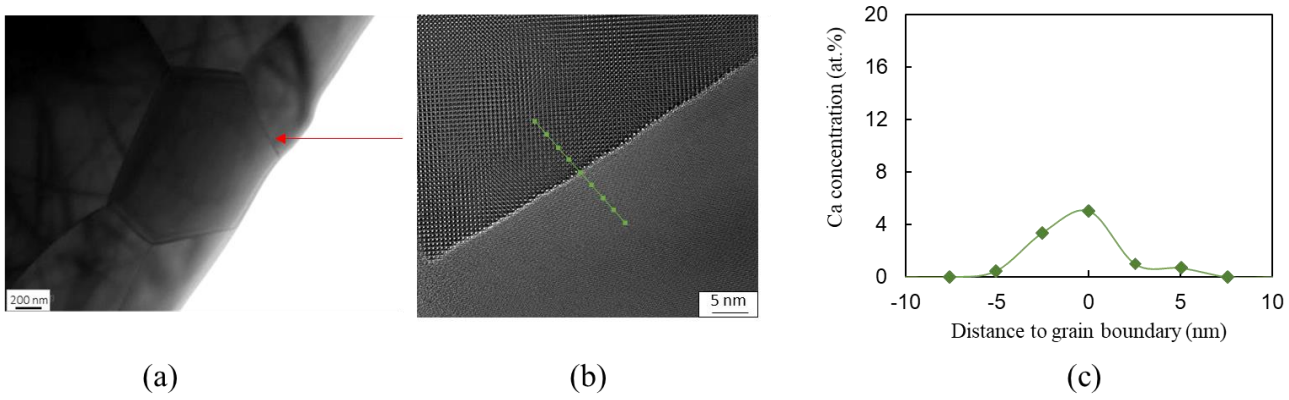

Figure 6 : TEM micrographs of CaMg1300 sample and corresponding STEM chemical analysis profile showing Ca segregation at grain boundaries.

Samples were then chemically analyzed thanks to NanoSIMS allowing to determine the spatial distribution of each dopants (Ca, Mg and Cr, *cf.* Figure 7) with much more sensitivity than previous STEM analyses. It is clear from these analyses that Ca and Mg are present with overconcentration at grain boundaries. On the contrary, Cr appear to be homogeneously distributed at nano- and micrometric scale in Ca,Mg,Cr:YAG ceramics. Also from Y and Al detection, no significant enrichment or depletion of the main YAG matrix elements was detected. From TEM, STEM and NanoSIMS analyses, it can be concluded that Cr enters homogeneously in solid solution in YAG matrix, whereas Ca and Mg segregate in the vicinity of the grain boundaries by solid-solution enrichment of the YAG phase.

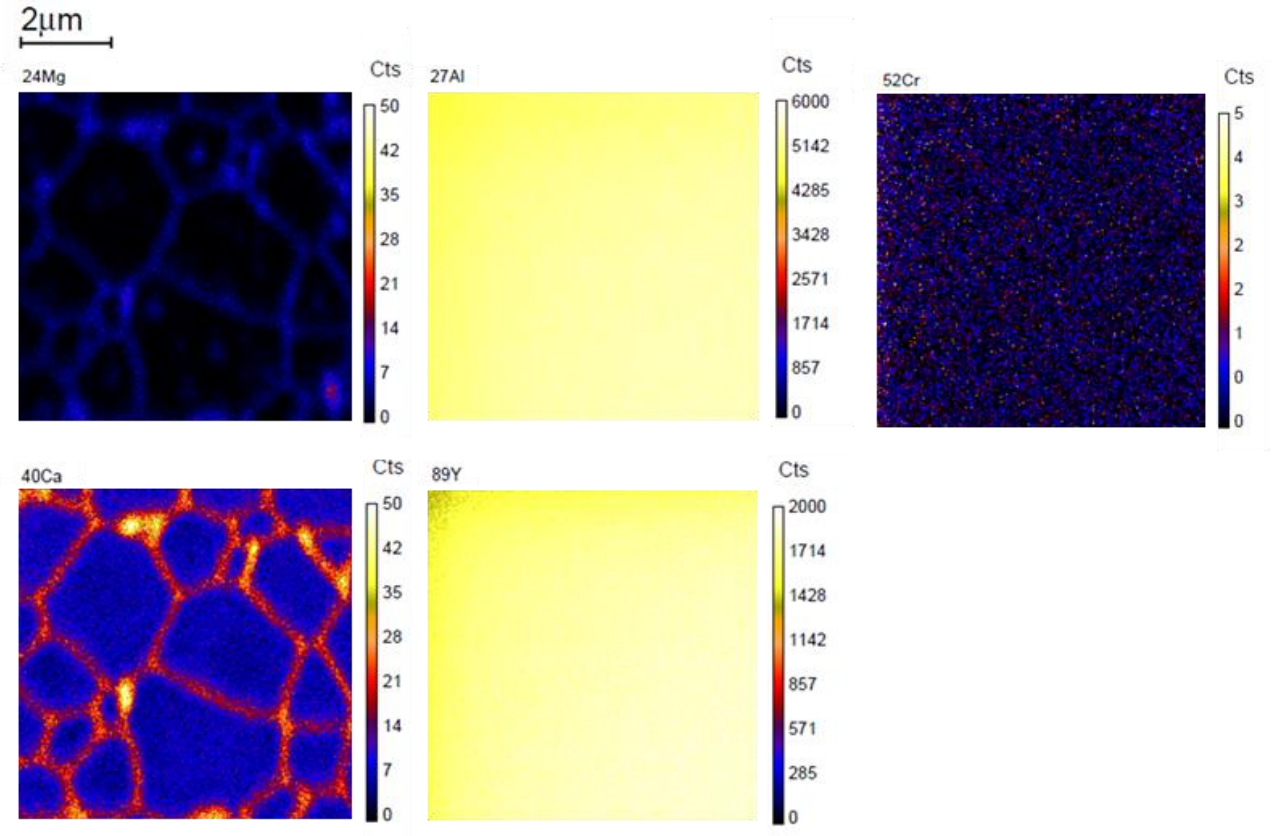

Figure 7: NanoSIMS micrographs of sintered samples CaMg1300 showing the spatial distribution of major (Y, Al) and minor (Cr, Mg, Ca) elements.

3.2. *Analyses of Cr^{3+} and Cr^{4+} concentration and distribution*

At first, Cr:YAG samples were annealed in order to obtain Cr^{4+}:YAG transparent ceramics. Chromium oxidation was monitored by measuring the optical transmission spectrum before and after air annealing. Comparison of transmission spectra of Cr:YAG ceramics after vacuum sintering and after air annealing (Figure 8) shows important change of absorption bands that can be attributed to the valence conversion of chromium [5]. The two absorption bands with maxima near 430 nm and 600 nm in the Cr:YAG as-sintered ceramic are attributed respectively to the $^4A_2 \rightarrow {}^4T_1$ and $^4A_2 \rightarrow {}^4T_2$ transitions of Cr^{3+}. After air annealing treatment, the color of ceramics changed from green to brown (view of samples in Figure 2) due to the presence of two broad absorption bands from 800 nm to 1200 nm and from 300 nm to 600 nm attributed respectively to tetravalent chromium in tetrahedral and octahedral sites. The intensities of the absorption bands attributed to Cr^{4+} vary if the sample contains Si element or not Figure 8). In the presence of silicon (sample CaMgSi1300), a decrease in the intensity of the two

absorption bands attributed to Cr^{4+} and a lighter brown color (Figure 2) indicate a lower $Cr^{3+} \rightarrow Cr^{4+}$ conversion than for the sample without Si (CaMg1300).

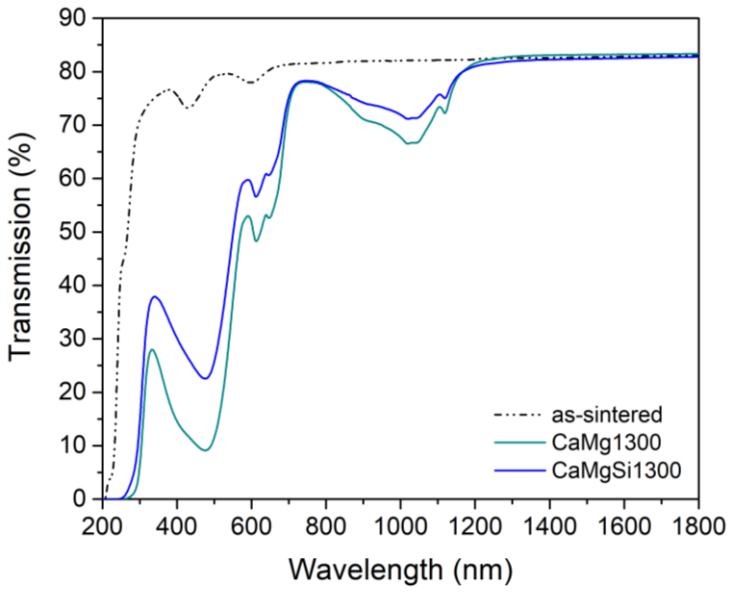

Figure 8: Transmittance spectra for Cr:YAG transparent ceramics before (as-sintered) and after air annealing at 1300°C.

The Cr^{4+} concentration of Cr:YAG samples were calculated by Eq. (1) and the values listed in Table 1 were compared to those measured for a Cr^{4+}:YAG single-crystal. The obtained results show higher values of the ratio Cr^{4+}/Cr_{total} with the elevation of annealing temperature for ceramics. For the same annealing conditions, the sample with silicon (CaMgSi1300) shows a lower $[Cr^{4+}]/[Cr_{total}]$ ratio than the sample without this element (CaMg1300). Finally, Table 3 shows a higher Cr^{4+}/Cr_{total} concentration ratio for all ceramic samples compared to single crystal.

Table 2 : Spectroscopic characteristics of 0.1at.%Cr^{4+}:YAG ceramics and single-crystal.

Sample	Transmittance at 1064 nm T/T_{max} (%)	Attenuation coefficient at 1064 nm (cm^{-1})	$[Cr^{4+}]$ ($ions.cm^{-3}$)	$[Cr^{4+}]$ (at.%)	Cr^{4+}/Cr_{total} convertion ratio
CaMg1200	87.6	2.28	$4.53 \cdot 10^{18}$	0.0197	19.7
CaMg1300	80.7	3.02	$6.00 \cdot 10^{18}$	0.0260	26.0
CaMgSi1300	85.3	2.17	$4.31 \cdot 10^{18}$	0.0187	18.7
Single-crystal	89.9	1.78	$3.53 \cdot 10^{18}$	0.0153	15.3

In order to complete these results, samples were characterized in terms of homogeneity by LSFI adapted to the fluorescence of Cr^{4+} ions. Results are reported in Figure 9 and show different fluorescence zones analysed by LSFI in CaMg1200 sample. After correction of the spatial distribution of deposited energy

(paraboloid), the fluorescence intensity profiles obtained show a fairly uniform shape without strong local or global divergence. As a conclusion, Cr^{4+}:YAG ceramic samples are homogeneous at macrometric scale with local Cr^{4+} concentration variations < 2% (*i.e.* below the detection limit of the apparatus).

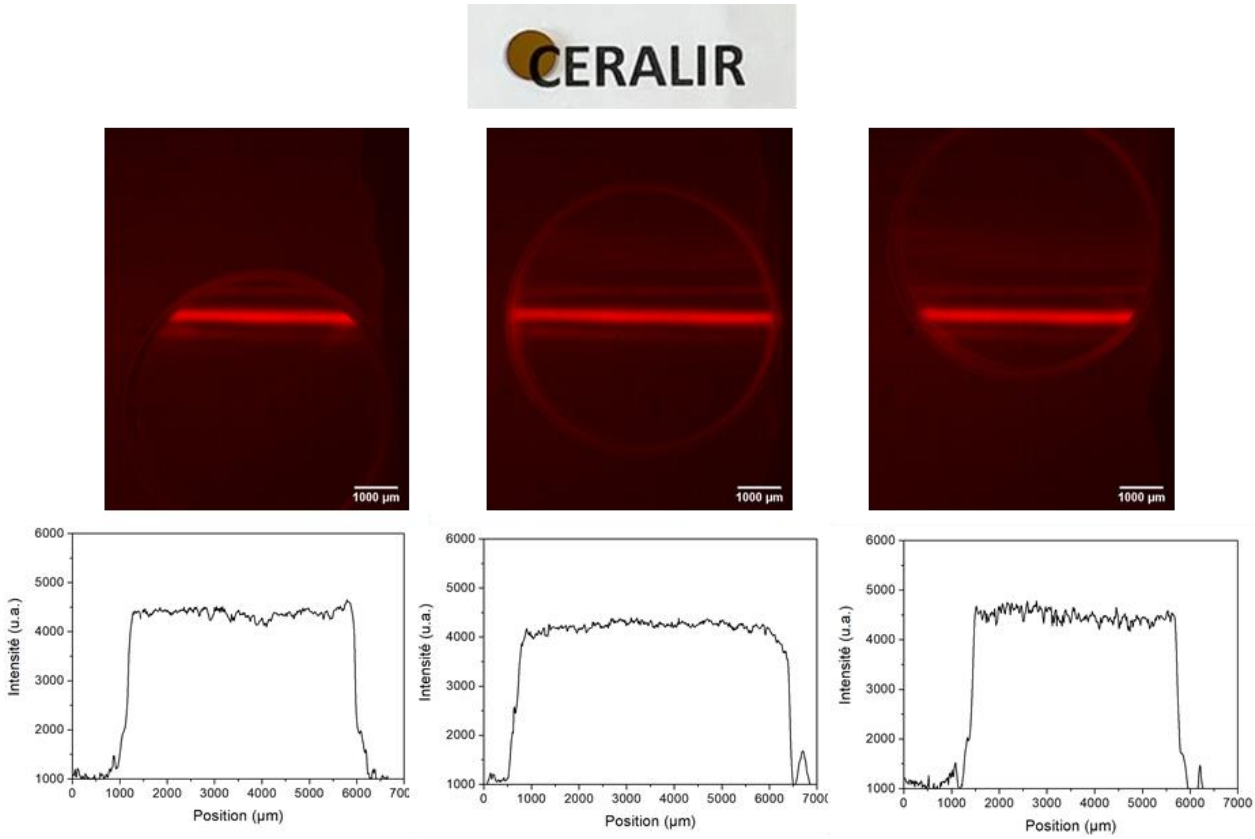

Figure 9: LSFI characterization of Cr^{4+}:YAG transparent ceramics (sample CaMg1200).

3.3. *Evaluation of performances as saturable absorber*

Performance of Cr^{4+}:YAG ceramic as SA was measured and compared to single crystal ones. Figure 10 reports the evolution of transmission at 1064 nm as a function of peak fluence. The different Cr^{4+}:YAG samples display the optical behavior of a saturable absorber: the absorption of light decreases with the increasing of light intensity. The fluence value at which the component no longer absorbs corresponds to its saturation fluence. Low saturation fluence has the advantage that the laser mode-locking can be started at low power level. This avoids a fast SA degradation.

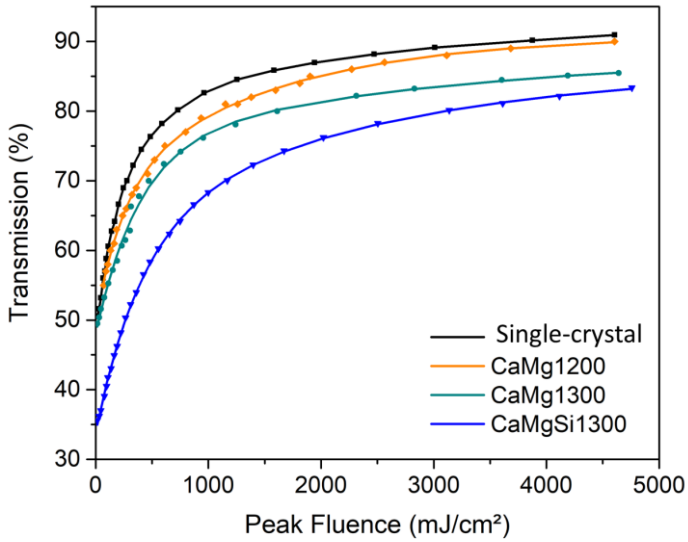

Figure 10: Transmission at 1064 nm as a function of peak fluence for Cr^{4+}:YAG ceramics in comparison to standard single-crystal.

F_{sat}, T_0 and T_{max} values are summarized in Table 3. The ground-state absorption cross-sections were calculated following the Eq. (6).

$$\sigma_{gs} = \frac{h \times \nu}{\lambda \times F_{sat}} \qquad (6)$$

where h is the Plank's constant, ν is the frequency of the incident radiation and F_{sat} is the saturation

$\sigma gs \sigma es = ln T0 / ln T max$

(2). On one hand, Table 3 shows that Cr^{4+}:YAG single-crystal have a lower saturable fluence and σ_{esa} values than ceramics ones. On the other hand, it appears that addition of silicon in the Cr:YAG ceramics composition causes an increase in saturation fluence value.

Table 3: Laser properties of Cr^{4+}:YAG samples.

Sample	Initial transmittance at 1064 nm T_0 (%)	Max. transmittance at 1064 nm T_{max} (%)	F_{sat} ($J.m^{-2}$)	σ_{gsa} (m^2)	σ_{esa} (m^2)	Laser pulse energy (mJ)	Laser pulse duration (ns)
Single-crystal	50.0	96.4	2730	$6.84.10^{-23}$	$3.62.10^{-24}$	49	16
CaMg1200	49.3	92.3	4500	$4.15.10^{-23}$	$4.70.10^{-24}$	38.8	45
CaMg1300	49.5	91.6	3790	$4.93.10^{-23}$	$6.15.10^{-24}$	-	-
CaMgSi1300	35.6	91.5	4420	$4.23.10^{-23}$	$3.64.10^{-24}$	-	-

Finaly, the laser performance of the Cr^{4+}:YAG ceramics with higher transmission (CaMg1200) were compared to single-crystal ones. The study revealed close laser pulse durations and laser average

energies generated between the two families of material (Table 3). With single crystal as the saturable absorber, the average generated energy measured was 44 mJ with a pulse duration of 33 ns while the values were 38.8 mJ and 45 ns respectively for the ceramic component. Thus, Cr^{4+}:YAG ceramics operated with only a 12% of decrease in energy output compared to commercial single crystal. This slight decrease in performance can be easily explained by the higher saturation fluence and the lower final transmission observed in the case of ceramic.

4. Discussion

At first, this study focused on the characterization of the microstructure of Cr:YAG ceramics, in particular with regards to the grain size and the distribution of dopants. Interestingly, very limited difference of grain size is observed in the case of Si addition or not. According to the literature, Si is well known to promote densification and grain growth in YAG ceramics, and is usually used to obtain highly transparent ceramics [39,40]. On the contrary, Ca was reported to strongly limit grain growth [15,17,19]. From STEM and NanoSIMS analyses, it was evidenced a segregation of Ca and Mg at grain boundaries but no extra-phase was detected. Thus, Ca and Mg segregate in the vicinity of the grain boundaries by solid-solution enrichment of the YAG phase. On the contrary, Cr appear to be homogeneously distributed at nano- and micrometric scale. To explain such difference in segregation behaviour, one have to consider the difference of valence between the cations. Ca^{2+} and Mg^{2+} are aliovalent, requiring oxygen vacancies as charge compensating defect, and Cr^{3+} being isovalent, requiring no compensating defects (it is expected that chromium ions occur only in the valence state +III during vacuum sintering as it is a sufficiently reducing atmosphere). Moreover, despite a 15% size difference from that of the host ion (Al in the octahedral site), chromium did not segregate. These results are in accordance with the works of Brown *et al.* showing Ca segregation and no Cr segregation at [111] orientated surfaces of YAG single-crystals [41]. According to their works and our results, it seems that this difference in surface enrichment (here grain boundaries) is linked to variations in valence and could be correlated to complex chemical/structural arrangement at the grain boundaries due to dopant

segregation and associated charge compensation defects. Thanks to these first experiments, it appears that calcium and magnesium addition inhibits the effect of Si on grain growth in YAG ceramics. It can be deduced from this observation that the Ca-rich layer at the grain boundaries decreases the mass transfer across grain boundaries. This phenomenon leads to a decrease of the grain boundary migration rate. This process results in a decrease in grain size, leading to Cr,Ca,Mg:YAG ceramics with an average grain size around ten times lower than ceramics usually sintered with only Si addition. Owing to this difference in concentration of divalent dopants in the vicinity of grain boundaries, chromium environment can be disturbed and could have an effect on Cr^{3+} to Cr^{4+} conversion efficiency during annealing.

Regarding the optical properties of Cr^{4+}:YAG ceramics, especially the optical absorption and the Cr^{4+}/Cr_{total} ratio, the obtained results first show higher values of the ratio Cr^{4+}/Cr_{total} with the elevation of annealing temperature for ceramics. Such result has been already observed in previous studies [29,32,42], showing that the conversion kinetics of Cr^{4+} ion significantly increases by increasing temperature and/or oxygen partial pressure. Nevertheless, the maximum concentration ratio between Cr^{3+} and Cr^{4+} seems to be largely lower than 100% even for high annealing time and/or temperature. The conversion efficiency is generally around 30-50% [17,28]. Second, for the same annealing conditions, the sample with silicon (CaMgSi1300) shows a lower $[Cr^{4+}]/[Cr_{total}]$ ratio than the sample without this element (CaMg1300). In YAG matrix, silicon substitutes on tetrahedral Al sites because of the similar ionic radii of Si^{4+} (r = 0.026 nm) and tetrahedral Al^{3+} (r = 0.039 nm) [43]. Si^{4+} and Cr^{4+} takes the same position in YAG structure and the competition between these two cations can explain the reduction of chromium conversion in +IV valence state. Also, Si^{4+} can limit the charge compensating effect of divalent ions. Third, a higher Cr^{4+}/Cr_{total} concentration ratio is observed for all ceramic samples compared to single crystal. According to Shan *et al.* [10], this better conversion could be attributed to the presence of grain boundaries in ceramics. In their study, they consider the grain boundaries as rapid channels for the diffusion of oxygen atoms and thus they cause an acceleration of the oxidation of chromium. Also for the authors, the solubility of divalent ions (Ca^{2+} and Mg^{2+}) is higher and more

homogeneous for ceramics than for single crystals, which can be beneficial for the conversion of tetravalent Cr ions. Our results provide some additional ideas. Especially, it was shown that Ca^{2+} and Mg^{2+} divalent ions segregate at grain boundaries on the contrary to chromium, leading to a higher (Ca+Mg)/Cr concentration ratio in the vicinity of grain boundaries. As a result, Cr^{3+} to Cr^{4+} conversion efficiency could be promoted. From LSFI fluorescence analyses, it is clear that this effect is spatially limited and does not lead to a strong variation of Cr^{4+} concentration at micrometric or larger scale. Complementary analyses aimed at deeper investigation of Cr^{4+} concentration gradient at grain boundaries, *e.g.* by fluorescence microscopy, should be useful.

Finally, laser performance of Cr^{4+}:YAG ceramics used as SA were comparable to single-crystal one in terms of energy. Nevertheless, the pulse duration remains significantly lower. On one hand, one have to point out that the choice of crystallographic orientation of single crystals can promote transmission and SA properties, whereas randomly oriented grains on ceramics doesn't permit this adjustment setting [44]. This can explain a part of the difference observed between single-crystal and polycristalline ceramic samples. Also, it can be concluded that the amount of light scattering in ceramic samples should be pretty low. This is in accordance with the almost defect-free microstructure of Cr:YAG ceramics as observed by SEM or TEM. Compared to Si, Ca strongly decreases grain growth kinetics during sintering, which is well known to be favorable to obtain full densification, *i.e.* the total elimination of porosity. Thus, when Cr:YAG ceramics are doped with an appropriate amount of Ca, *i.e.* below the solubility limit but sufficient to make an efficient conversion of Cr^{3+} to Cr^{4+}, fully dense and transparent ceramics can be obtained after sintering. On the other hand, it appears that addition of silicon on the ceramic composition causes an increase in saturation fluence value. This result can be directly correlated to the lower chromium conversion rate when Si is added as a codopant in YAG. This study confirms that silicon should be excluded for the manufacturing of transparent Cr^{4+}:YAG ceramics as SA. These results illustrate the complex interactions between dopants and demonstrate the need for a doping engineering approach with a multidisciplinary approach.

Conclusions

Polycristalline ceramics of Cr^{4+},Ca,Mg:YAG with high optical quality were synthesized by solid-state reactive sintering at 1750°C in vacuum. First, their microstructural and chemical features were investigated by HRTEM, STEM, NanoSIMS, optical transmittance spectroscopy and LSFI. In-line transmittance of the ceramics after vacuum sintering was 82.1% at λ = 1064 nm that is close to the theoretical limit including multiple reflections. Samples show a homogeneous microstructure with small grain size of about 2.9 to 2.4 µm in diameter, depending on Si addition or not, respectively. Calcium and magnesium segregation at grain boundaries was revealed by STEM and NanoSIMS whereas no segregation of chromium was observed. The limited grain growth during sintering was attributed to Ca and Mg segregation at grain boundaries, and is almost unaffected by the presence of Si. Nevertheless, Silicon addition decreases chromium conversion from Cr^{3+} to Cr^{4+} during annealing. The LSFI did not reveal any significant heterogeneity in the whole sample volume with respect to the valence state of the chromium after annealing.

Finally, the saturation fluence of Cr^{4+}:YAG ceramic samples was measured and samples were tested in a Q-switched Nd:YAG laser. A saturation fluence of 4500 $J.m^{-2}$, laser pulse energy of 38.8 mJ with pulse duration of 45 ns (*i.e.* power around 0.8 MW per pulse) were measured that is until now the most powerful laser demonstration using a Cr^{4+}:YAG polycristalline ceramic as saturable absorber.

Acknowledgments

The authors would like to thank CILAS company and DGA (French armaments procurement agency) for funding. This work was also supported by institutional grant from the National Research Agency under the Investments for the future program with the reference ANR-10-LABX-0074-01 Sigma-LIM. The authors would like to thank J. Aleon, S. Mostefaoui and M. Verdier (IMPMC, UMR CNRS 7590, Paris, France) for conducting NanoSIMS analyses and P. Carles (IRCER, UMR CNRS 7315, Limoges, France) for TEM and STEM analyses.

Bibliography

[1] Y. Li, W. Wang, S. Zhang, X. Zhang, Z. Liu, Z. Jiang, S. Li, Z. Liu, A novel La3Ga5SiO14 electro-optic Q-switched Nd:LiYF (Nd:YLF) laser with a Cassegrain unstable cavity, Optics Communications, 244 [1] (2005) 333-338. https://doi.org/10.1016/j.optcom.2004.09.048

[2] Q. Li, Y. Zheng, Z. Wang, T. Zuo, A novel high-peak power double AO Q-switches pulse Nd:YAG laser for drilling, Optics & Laser Technology, 14 (2005) 9-11. https://doi.org/10.1016/j.optlastec.2004.05.002

[3] O. Sandu, G. Salamu, N. Pavel, T. Dascalu, D. Chuchumishev, A. Gaydardzhiev, I. Buchvarov, High-peak power, passively Q-switched, composite, all-polycrystalline ceramic Nd : YAG/Cr 4+ :YAG lasers, Quantum Electron. 42 (2012) 211–215. https://doi.org/10.1070/QE2012v042n03ABEH014745.

[4] J. Tang, Z. Bai, D. Zhang, Y. Qi, J. Ding, Y. Wang, Z. Lu, Advances in All-Solid-State Passively Q-Switched Lasers Based on Cr4+:YAG Saturable Absorber, Photonics. 8 (2021) 93. https://doi.org/10.3390/photonics8040093.

[5] R. Feldman, Y. Shimony, Z. Burshtein, Dynamics of chromium ion valence transformations in Cr,Ca:YAG crystals used as laser gain and passive Q-switching media, Optical Materials. 24 (2003) 333–344. https://doi.org/10.1016/S0925-3467(03)00146-0.

[6] J. Dong, P. Deng, Y. Liu, Y. Zhang, J. Xu, W. Chen, X. Xie, Passively Q-switched Yb:YAG laser with Cr4+ :YAG as the saturable absorber, Applied Optics, 40 [24] (2001) 4303-4307. https://doi.org/10.1364/AO.40.004303

[7] Y. Kalisky, Cr4+-doped crystals: their use as lasers and passive Q-switches, Progress in Quantum Electronics. 28 [5] (2004) 249–303 https://doi.org/10.1016/j.pquantelec.2004.09.001.

[8] X. Xu, Z. Zhao, P. Song, G. Zhou, J. Xu, P. Deng, Effects of growth atmosphere, annealing temperature, Cr content, and Ca/Cr ratio on the Cr4+ absorption of Cr, Yb:YAG crystals, 21 [7] (2004) 1289-1293. https://doi.org/10.1364/JOSAB.21.001289

Ubiskii
[9] S.B. ~~Ubiskij~~ja, Chromium recharging processes in the $Y_3A1_50_{12}$: Mg, Cr single crystal under the reducing and oxidizing annealing influence, 4412 International Conference on Solid State Crystals 2000, Zacopane, Poland (2000) ADA399287. https://doi.org/10.1117/12.435801

[10] Y. SHAN, L. ZHANG, T. ZHOU, C. SHAO, L. ZHANG, Y. MA, YAO QING, SELIM F. A, CHEN H, One-order-higher Cr^{4+} conversion efficiency in Cr^{4+}:YAG transparent ceramics for a high-frequency passively Q-switched laser, Photonics Research. 7 [8] (2019) 933–938. https://doi.org/10.1364/PRJ.7.000933

[11] A. Sugimoto, Y. Nobe, K. Yamagishi, Crystal growth and optical characterization of Cr,Ca : $Y_3Al_50_{12}$, 140 [3-4] (1994) 349-354. https://doi.org/10.1016/0022-0248(94)90309-3

[12] S.A. Markgraf, M.F. Pangborn, R. Dieckmann, Influence of different divalent co-dopants on the Cr4 + content of Cr-doped $Y_3Al_5O_{12}$, Journal of Crystal Growth. 180 (1997) 81–84. https://doi.org/10.1016/s0022-0248(97)00158-9

[13] A. Ikesue, Y.L. Aung, Ceramic laser materials, Nature Photonics. 2 (2008) 721-727. https://doi.org/10.1038/nphoton.2008.243

[14] A. Goldstein, A. Krell, Z. Burshtein, Transparent ceramics: materials, engineering, and applications, First edition, John Wiley & Sons, Inc, Hoboken, New Jersey, 2020.

[15] L. Zhang, T. Zhou, F.A. Selim, H. Chen, Single CaO accelerated densification and microstructure control of highly transparent YAG ceramic, Journal of the American Ceramic Society. 101 [2] (2018) 703–712. https://doi.org/10.1111/jace.15233.

[16] M.A. Chaika, O.M. Vovk, A.G. Doroshenko, V.K. Klochkov, P.V.Mateychenko, S.V. Parkhomenko, O.G. Fedorov, Influence of Ca and Mg doping on the microstructure and optical properties of YAG ceramics., Functional Materials. 24 [2] (2017) 237–243. https://doi.org/10.15407/fm24.02.237.

[17] M.A. Chaika, P. Dluzewski, K. Morawiec, A. Szczepanska, K. Jablonska, G. Mancardi, R. Tomala, D. Hreniak, W. Strek, N.A. Safronova, A.G. Doroshenko, S.V. Parkhomenko, O.M. Vovk, The

role of Ca^{2+} ions in the formation of high optical quality Cr^{4+},Ca:YAG ceramics, Journal of the European Ceramic Society. 39 [11] (2019) 3344–3352. https://doi.org/10.1016/j.jeurceramsoc.2019.04.037.

[18] M.A. Chaika, G. Mancardi, O.M. Vovk, Influence of CaO and SiO_2 additives on the sintering behavior of Cr,Ca:YAG ceramics prepared by solid-state reaction sintering, Ceramics International. 46 [14] (2020) 22781–22786. https://doi.org/10.1016/j.ceramint.2020.06.045.

[19] T. Hua, Q. Zeng, J. Qi, G. Cheng, X. Chen, Z. Huang, Q. Zhang, X. Huang, X. Guo, N. Wei, T. Lu, Effect of calcium oxide doping on the microstructure and optical properties of YAG transparent ceramics, Mater. Res. Express. 6 [3] (2018) 036203. https://doi.org/10.1088/2053-1591/aaf487.

[20] T. Zhou, L. Zhang, Z. Li, S. Wei, J. Wu, L. Wang, H. Yang, Z. Fu, H. Chen, D. Tang, C. Wong, Q. Zhang, Toward vacuum sintering of YAG transparent ceramic using divalent dopant as sintering aids: Investigation of microstructural evolution and optical property, Ceramics International. 43 [3] (2017) 3140–3146. https://doi.org/10.1016/j.ceramint.2016.11.131.

[21] A.G. Doroshenko, R.P. Yavetskiy, S.V. Parkhomenko, I.O. Vorona, O.S. Kryzhanovska, P.V. Mateychenko, A.V. Tolmachev, E.A. Vovk, V.A. Bovda, G. Croitoru, L. Gheorghe, Effect of the sintering temperature on the microstructure and optical properties of YAG:Cr,Mg ceramics, Optical Materials. 98 (2019) 109505. https://doi.org/10.1016/j.optmat.2019.109505.

[22] I. Vorona, A. Balabanov, M. Dobrotvorska, R. Yavetskiy, O. Kryzhanovska, L. Kravchenko, S. Parkhomenko, P. Mateychenko, V. Baumer, I. Matolínová, Effect of MgO doping on the structure and optical properties of YAG transparent ceramics, Journal of the European Ceramic Society. 40 (2020) 861–866. https://doi.org/10.1016/j.jeurceramsoc.2019.10.048.

[23] A.A. Kravtsov, M.S. Nikova, D.S. Vakalov, V.A. Tarala, I.S. Chikulina, F.F. Malyavin, O.M. Chapura, S.O. Krandievsky, D.S. Kuleshov, V.A. Lapin, Combined effect of MgO sintering additive and stoichiometry deviation on YAG crystal lattice defects, Ceramics International. 45 [16] (2019) 20178–20188. https://doi.org/10.1016/j.ceramint.2019.06.287.

[24] T. Zhou, L. Zhang, S. Wei, L. Wang, H. Yang, Z. Fu, H. Chen, F.A. Selim, Q. Zhang, MgO assisted densification of highly transparent YAG ceramics and their microstructural evolution, Journal of the European Ceramic Society. 38 [2] (2018) 687–693. https://doi.org/10.1016/j.jeurceramsoc.2017.09.017.

[25] Y.C. Li, W. Guo, T.C. Lu, S.H. Tong, R.X. Fang, H. Xu, Sintering of Transparent Polycrystal Nd:YAG with MgO as Additive, Key Engineering Materials. 368–372 (2008) 426–428. https://doi.org/10.4028/www.scientific.net/KEM.368-372.426.

[26] T. Zhou, L. Zhang, H. Yang, X. Qiao, P. Liu, D. Tang, J. Zhang, Effects of Sintering Aids on the Transparency and Conversion Efficiency of Cr^{4+} Ions in Cr: YAG Transparent Ceramics, Journal of the American Ceramic Society. 98 [8] (2015) 2459–2464. https://doi.org/10.1111/jace.13616.

[27] T. Zhou, L. Zhang, J. Zhang, H. Yang, P. Liu, Y. Chen, X. Qiao, D. Tang, Improved conversion efficiency of Cr^{4+} ions in Cr: YAG transparent ceramics by optimization the particle sizes of sintering aids, Optical Materials. 50 (2015) 11–14. https://doi.org/10.1016/j.optmat.2015.07.037.

[28] V.V. Bezotosnyi, A.Y. Kanaev, Yu.L. Kopylov, A.L. Koromyslov, K.V. Lopukhin, I.M. Tupitsyn, E.A. Cheshev, Influence of CaO/MgO ratio on Cr3+ to Cr4+conversion efficiency in YAG:Cr4+ ceramic saturable absorbers, Optical Materials. 100 (2020) 109671. https://doi.org/10.1016/j.optmat.2020.109671.

[29] H. Yagi, K. Takaichi, K. Ueda, T. Yanagitani, A.A. Kaminskii, Influence of annealing conditions on the optical properties of chromium-doped ceramic $Y_3Al_5O_{12}$, Optical Materials. 29 (2006) 392–396. https://doi.org/10.1016/j.optmat.2005.08.035.

[30] K. Takaichi, J. Lu, T. Murai, T. Uematsu, A. Shirakawa, K.-I. Ueda, H. Yagi, T. Yanagitani, A.A. Kaminskii, Chromium doped $Y_3Al_5O_{12}$ ceramics - A novel saturable absorber for passively self-Q-switched one-micron solid state lasers, J. J. Appl. Phys., Part 2. 41 (2002). https://doi.org/10.1143/JJAP.41.L96

[31] M. Chaika, W. Paszkowicz, W. Strek, D. Hreniak, R. Tomala, N. Safronova, A. Doroshenko, S. Parkhomenko, P. Dluzewski, M. Kozłowski, O. Vovk, Influence of Cr doping on the phase composition of Cr,Ca:YAG ceramics by solid state reaction sintering, Journal of the American Ceramic Society. 102 [4] (2019) 2104–2115. https://doi.org/10.1111/jace.16024.

[32] M.A. Chaika, R. Tomala, W. Strek, D. Hreniak, P. Dluzewski, K. Morawiec, P.V. Mateychenko, A.G. Fedorov, A.G. Doroshenko, S.V. Parkhomenko, K. Lesniewska-Matys, D. Podniesinski, A. Kozłowska, G. Mancardi, O.M. Vovk, Kinetics of Cr^{3+} to Cr^{4+} ion valence transformations and intra-lattice cation exchange of Cr^{4+} in Cr,Ca:YAG ceramics used as laser gain and passive Q-switching media, J Chem Phys. 151 (2019) 134708. https://doi.org/10.1063/1.5118321.

[33] R. Boulesteix, C. Chevarin, R. Belon, A. Maître, L. Cochain, C. Sallé, Manufacturing of Large Size and Highly Transparent Nd:YAG Ceramics by Pressure Slip-Casting and Post-Sintering by HIP: An Experimental and Simulation Study, Materials. 13 [9] (2020) 2199. https://doi.org/10.3390/ma13092199.

[34] M.M. Kuklja, Defects in yttrium aluminium perovskite and garnet crystals: atomistic study, J. Phys.: Condens. Matter. 12 (2000) 2953–2967. https://doi.org/10.1088/0953-8984/12/13/307.

[35] L. Schuh, R. Metselaar, G. de With, Electrical transport and defect properties of Ca- and Mg-doped yttrium aluminum garnet ceramics, Journal of Applied Physics. 66 (1989) 2627–2632. https://doi.org/10.1063/1.344485.

[36] R. Boulesteix, C. Perrière, A. Maître, L. Chrétien, A. Brenier, Y. Guyot, Fabrication of YAG/Cr:YAG transparent composite ceramics and characterization by light sheet fluorescence imaging, Optical Materials. 96 (2019) 109324. https://doi.org/10.1016/j.optmat.2019.109324.

[37] Y. Kalisky, A. Ben-Amar Baranga, Y. Shimony, Z. Burshtein, S.A. Pollack, M.R. Kokta, Cr^{4+} doped garnets: their properties as non-linear absorbers, Optical Materials. 6 (1996) 275–280. https://doi.org/10.1016/S0925-3467(96)00053-5.

[38] Z. Burshtein, P. Blau, Y. Kalisky, Y. Shimony, M.R. Kikta, Excited-state absorption studies of Cr^{4+} ions in several garnet host crystals, IEEE J. Quantum Electron. 34 [2] (1998) 292–299. https://doi.org/10.1109/3.658716.

[39] S. Kochawattana, A. Stevenson, S.-H. Lee, M. Ramirez, V. Gopalan, J. Dumm, V.K. Castillo, G.J. Quarles, G.L. Messing, Sintering and grain growth in SiO_2 doped Nd:YAG, Journal of the European Ceramic Society. 28 [7] (2008) 1527–1534. https://doi.org/10.1016/j.jeurceramsoc.2007.12.006.

[40] A.J. Stevenson, X. Li, M.A. Martinez, J.M. Anderson, D.L. Suchy, E.R. Kupp, E.C. Dickey, K.T. Mueller, G.L. Messing, Effect of SiO_2 on Densification and Microstructure Development in Nd:YAG Transparent Ceramics, Journal of the American Ceramic Society. 94 [5] (2011) 1380–1387. https://doi.org/10.1111/j.1551-2916.2010.04260.x.

[41] K.R. Brown, D.A. Bonnell, Segregation in yttrium aluminum garnet: I, experimental determination, J. Am. Ceram. Soc. 82 [9] (1999) 2423–2430.

[42] T. Zhou, L. Zhang, Z. Li, S. Wei, J. Wu, L. Wang, H. Yang, Z. Fu, H. Chen, C. Wong, Q. Zhang, Enhanced conversion efficiency of Cr^{4+} ion in Cr: YAG transparent ceramic by optimizing the annealing process and doping concentration, Journal of Alloys and Compounds. 703 (2017) 34–39. https://doi.org/10.1016/j.jallcom.2017.01.338.

[43] R. D. SHANNON, Revised Effective Ionic Radii and Systematic Studies of Interatomie Distances in Halides and Chaleogenides, Acta Crystallographica. 32 [5] (1976) 751–767. https://doi.org/10.1107/S0567739476001551

[44] H. Sakai, A. Sone, H. Kan, T. Taira, Polarization stabilizing for diode-pumped passively Q-switched Nd:YAG microchip lasers, in: Advanced Solid-State Photonics, OSA, Incline Village, Nevada, 2006: p. MD2. https://doi.org/10.1364/ASSP.2006.MD2.